Meta-analysis reveals host-dependent nitrogen recycling as a mechanism of symbiont control in *Aiptasia*

Guoxin Cui[1], Yi Jin Liew[1], Yong Li[1], Najeh Kharbatia[2], Noura I Zahran[1], Abdul-Hamid Emwas[2], Victor M Eguiluz[3], Manuel Aranda[1]*

[1]King Abdullah University of Science and Technology (KAUST), Red Sea Research Center (RSRC), Biological and Environmental Science & Engineering Division (BESE), Thuwal, 23955-6900, Saudi Arabia

[2]King Abdullah University of Science and Technology (KAUST), Core Labs, Thuwal, 23955-6900, Saudi Arabia

[3]Instituto de Física Interdisciplinar y Sistemas Complejos IFISC (CSIC-UIB), E-07122 Palma de Mallorca, Spain

* Correspondence to Manuel Aranda, manuel.aranda@kaust.edu.sa

Abstract

The metabolic symbiosis with photosynthetic algae of the genus *Symbiodinium* allows corals to thrive in the oligotrophic environments of tropical seas. Many aspects of this relationship have been investigated using transcriptomic analyses in the emerging model organism *Aiptasia*. However, previous studies identified thousands of putatively symbiosis-related genes, making it difficult to disentangle symbiosis-induced responses from undesired experimental parameters. Using a meta-analysis approach, we identified a core set of 731 high-confidence symbiosis-associated genes that reveal host-dependent recycling of waste ammonium and amino acid synthesis as central processes in this relationship. Combining transcriptomic and metabolomic analyses, we show that symbiont-derived carbon enables host recycling of ammonium into nonessential amino acids. We propose that this provides a regulatory mechanism to control symbiont growth through a carbon-dependent negative feedback of nitrogen availability to the symbiont. The dependence of this mechanism on symbiont-derived carbon highlights the susceptibility of this symbiosis to changes in carbon translocation, as imposed by environmental stress.

Introduction

The symbiotic relationship between photosynthetic dinoflagellates of the genus *Symbiodinium* and corals is the foundation of the coral reef ecosystem. This metabolic symbiosis is thought to enable corals to thrive in the oligotrophic environment of tropical oceans by allowing efficient recycling of nitrogenous waste products in return for photosynthates from the symbionts[1]. Despite the importance of this symbiotic relationship, research has been hampered by the general

39 difficulties associated with the maintenance of corals, their slow growth rates, and the
40 infeasibility of maintaining them in an aposymbiotic state[2].

41 To overcome these disadvantages, the sea anemone *Aiptasia* (sensu *Exaiptasia pallida*[3]) has
42 emerged as a powerful model system in the study of cnidarian-*Symbiodinium* symbiosis. *Aiptasia*
43 belongs to the same class (Anthozoa) as corals, and similarly establishes a symbiotic relationship
44 with *Symbiodinium*[4]. In contrast to corals, it can be easily maintained and effectively
45 manipulated under common laboratory conditions. Its rapid asexual reproduction provides
46 relatively large amounts of experimental material for high-throughput studies[5], while sexual
47 reproduction can be induced efficiently under well-designed conditions[6]. More importantly for
48 symbiosis-related studies, *Aiptasia* can be maintained in an unstressed, aposymbiotic state as
49 long as it is fed regularly[7, 8]. It can also be re-infected with a variety of *Symbiodinium* strains[9],
50 which allows for comparative studies analyzing the effects of different symbionts on the host.
51 The use of *Aiptasia* as a model organism has advanced our understanding of the metabolic
52 aspects of symbiosis, in particular the identification of glucose as the main metabolite transferred
53 from symbiont to host[10]. However, the molecular mechanisms underlying host-symbiont
54 metabolic interactions are still largely unknown. Particularly the role of nitrogen recycling from
55 waste ammonium is still debated. While it is generally assumed that ammonium assimilation is
56 predominantly performed by the symbiont, some studies show that symbiont-growth is nitrogen
57 limited *in hospite*[11, 12, 13, 14], suggesting that the host might be able to control nitrogen availability.
58 Consequently, it has been proposed that recycling of ammonium waste by the host might serve as
59 a mechanism to control symbiont densities[15, 16].

60 Many genomic, transcriptomic, and proteomic studies have been conducted on the topic of
61 cnidarian-*Symbiodinium* symbiosis in the last two decades to unravel the molecular

underpinnings of this relationship[17, 18, 19, 20, 21, 22, 23]. Due to technical limitations, most of these studies did not have the sensitivity required to detect extensive changes of symbiosis-associated genes. However, these limitations are gradually being overcome by next-generation sequencing techniques. The first *Aiptasia*-centered whole transcriptome comparison between symbiotic and aposymbiotic animals was performed by Lehnert et al.[24]. Since then, multiple studies on the *Aiptasia-Symbiodinium* symbiosis have explored different aspects of this relationship and raised several interesting hypotheses[2, 25]. Despite this increasing wealth of information, our knowledge of underlying key genes associated with this relationship is still limited. While transcriptomic studies have provided valuable information, the resulting lists of putative candidate genes contain thousands of genes, making it difficult to disentangle true symbiosis-related signals from other experimental and technical factors. Furthermore, it was difficult to contrast results across studies due to the lack of a reference genome when most of the studies were carried out. The recent availability of the *Aiptasia* genome[2] provides a set of high-quality gene models as a reference for transcriptomic analyses. RNA-Seq data can now be mapped directly to these gene models for quantification, thus allowing the comparison of results across different studies.

Here, we carried out a meta-analysis of four RNA-Seq datasets comparing expression differences between symbiotic and aposymbiotic *Aiptasia* (strain CC7) in order to discern sources of technical errors and experimental variations, and to identify a core set of genes and pathways involved in symbiosis establishment and maintenance.

Results

We conducted our meta-analysis on 3 previous RNA-Seq studies that generated 4 separate datasets, encompassing 17 biological replicates per symbiosis state (i.e., aposymbiotic and symbiotic)[2, 24, 26].

Batch effects. In this study, we focused solely on the annotated genes of the previously published *Aiptasia* genome[2]. To investigate the relationship between samples from different studies, we first performed a principal component analysis (PCA) and a rank correlation analysis (RCA) on inter-sample normalized transcripts per million (TPM) values. Both the PCA (Fig. 1A) and RCA (Fig. 1B) showed clear grouping of samples by experiment rather than symbiotic state. However, PCA performed on samples from individual studies showed a clear separation of the samples by symbiotic condition (Fig. S1**)**. This indicates that technical and/or experimental batch effects from each study exert stronger effects on gene expression profiles than the actual symbiotic state of the animals.

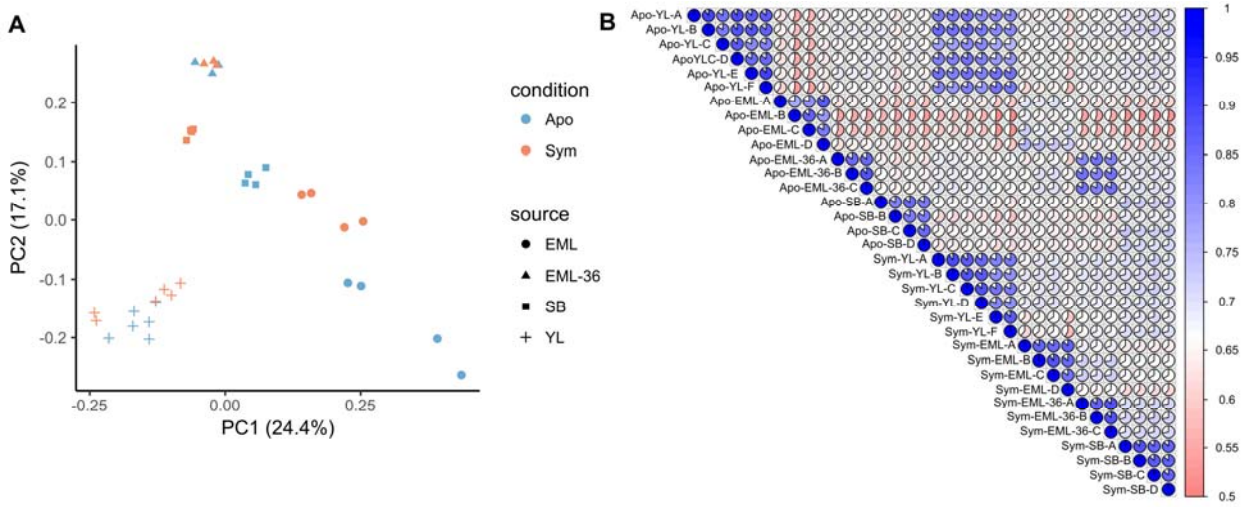

FIG 1 Relationship between samples from different studies. (A) Principal component analysis of samples across all four studies. The symbiotic state (condition) of the animals was indicated by the color of the points, while the source studies were represented as different shapes. (B) Kendall rank correlation of all samples, with high-correlation as blue, and low-correlation as red. The pie chart in each cell also indicates the correlation of the two samples from the corresponding row and column. In both figures, Apo and Sym represent the symbiotic state of the anemones: aposymbiotic and symbiotic, respectively. YL, SB, EML, and EML-36 are the initials of the first authors whose papers we obtained the RNA-Seq data (i.e. Yong Li[26], Sebastian Baumgarten[2], and Erik M. Lehnert[24], respectively).

Differential expression analyses. Although the four datasets were distinct, there was still a clear separation of symbiotic and aposymbiotic replicates within each of the datasets. We hypothesized that this separation was due to the differential expression of core genes involved in symbiosis initiation and/or maintenance. To identify these genes, we performed four independent differential expression analyses using the exact same pipeline and parameters. These analyses identified between 2,398 to 11,959 differentially expressed genes (DEGs), corresponding to ~10–50% of all expressed genes in the respective studies (Table 1). Surprisingly, the overlap between these lists of DEGs was poor despite the large number of DEGs identified in the individual analyses: only 300 genes were consistently differentially expressed across all four studies. Out of these 300 genes, 166 were upregulated in symbiotic anemones in all comparisons, while 134 were found to be downregulated in symbiotic animals, relative to aposymbiotic controls (Table 1). Paradoxically, we also found 93 genes of 393 genes (23.7%) that were

120 differentially expressed in all studies, but in different directions. At this point, we sought a better
121 technique to identify the core genes involved in symbiosis.

122

123 **TABLE 1** Number of differentially expressed genes in different analyses. "Upregulated" and
124 "downregulated" refers to the number of genes that are expressed at higher levels and lower
125 levels respectively in symbiotic *Aiptasia*, relative to aposymbiotic ones.

Study	Expressed	DEGs	Upregulated	Downregulated
YL	27,684	3,058	1,552	1,506
SB	24,013	11,959	6,072	5,887
EML	24,511	9,613	4,758	4,855
EML-36	24,246	2,398	1,241	1,157
Overlap	22,394	393	166	134
Meta-analysis	25,857	731	366	365

126

127

128 **Performing a meta-analysis across four datasets.** To obtain a more robust set of core genes
129 involved in symbiosis, we performed a meta-analysis with random effects across the four
130 independent differential gene expression analyses (Table S1). Using this approach, we identified
131 731 genes that exhibited a more consistent response to symbiosis.
132 To assess the robustness of these genes, we carried out a principal variance component analysis
133 (PVCA)[27] to detect the connections between the expression profiles and the different
134 experimental parameters used in each study (Fig. 2, Table S2). For the four individual studies,
135 we found that the symbiotic state of the anemones accounts for a relatively small fraction (6.5%
136 in raw data, 8.4% in normalized data) of the observed variance. Most of the variance was
137 introduced by differences in feeding frequency, days between feeding and sampling, water, light
138 intensity, and temperature. We further noticed that a large proportion of the variance across these
139 four datasets remained unaccountable, suggesting that technical variability, e.g. RNA extraction,

library preparation and sequencing, also introduces substantial unwanted heterogeneity to gene expression profiles. When the PVCA was similarly applied to the 731 genes identified through our meta-analysis, we observed that these genes had a significantly enhanced association with symbiosis. Symbiosis state accounted for 46.6% of the expression variance observed in these genes (Fig 2).

We noticed that smaller gene lists tended to have variances that were better explained by symbiosis state, exemplified by DEG_YL and DEG_EML-36 having better association with symbiosis than DEG_SB and DEG_EML. Thus, one could argue that the meta-analysis merely achieved better association with symbiosis as it had the fewest genes of interest. To assess this confounding factor, we performed PVCA on a set of randomly picked 731 genes from DEG_YL. This was repeated 10,000 times (i.e., a Monte-Carlo approach), and for other DEG lists (DEG_SB, DEG_EML and DEG_EML-36). These simulations allowed us to estimate that the likelihood of our meta-analysis producing the observed 46.6% by random chance was $p < 10^{-4}$ (0 of 40,000 trials had symbiosis state accounting for > 46.6% of the variance).

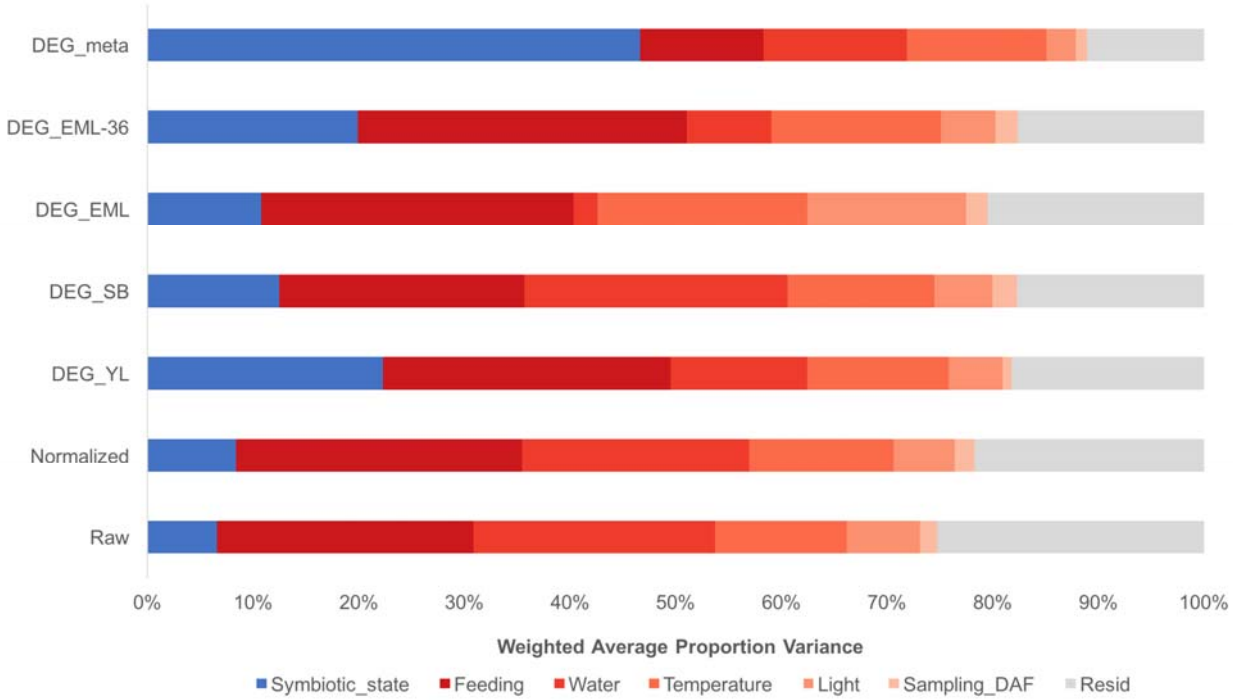

FIG 2 Principal variance component analysis of DEGs from different analyses. The contribution of each factor to the overall variance in each analysis was estimated by PVCA. The variance explained by symbiotic state (blue) is highest in the set of DEGs from the meta-analysis (DEG_meta); the combined variation attributable to experimental factors (red) is lowest in DEG_meta as well. Unresolved variance is in gray. DEG_YL, _SB, _EML and _EML-36 represents the set of differentially expressed genes identified in four independent differential analyses. Raw and Normalized are the combined raw and inter-sample normalized expression data across all *Aiptasia* genes, showing that < 10% of the variation in overall gene expression can be attributed to symbiotic state. DAF: days after feeding.

166 **Functional interpretation.** To assess the impact of the previously identified experiment-specific
167 biases, we conducted GO and KEGG pathway enrichment analyses on the DEGs identified using
168 the four independent differential gene expression analyses, respectively. Across the analyses of
169 four independent experiments, 283–645 GO terms and 9–55 KEGG pathways were enriched.
170 However, the functional overlap across all studies was poor: a large proportion of the putatively
171 enriched terms were only identified in a single dataset (~75% in GO, and ~65% in KEGG) (Fig.
172 S2). Compared to these independent analyses, the GO and KEGG pathway enrichment of the 731
173 symbiosis-associated core genes contained fewer significant GO terms (204), but comparatively
174 more significantly enriched KEGG pathways (31). Many of the enriched GO terms and KEGG
175 pathways, as well as their associated genes, fit well with processes previously reported to be
176 involved in symbiosis, including symbiont recognition and the establishment of symbiosis, host
177 tolerance of symbiont, and nutrient exchange between partners and host metabolism which are
178 discussed separately (Supplementary Information S1). However, our analysis also identified
179 several symbiosis-related processes that were previously overlooked; of these processes,
180 pathways associated with amino acid metabolism exhibited the most extensive changes in
181 response to symbiosis.

182 **Extensive changes of amino acid metabolism in response to symbiosis.** Amino acid and
183 protein metabolism represented a major symbiosis-related aspect in our meta-analysis. 9 of 31
184 enriched KEGG pathways and 18 of 125 enriched biological process GO terms were associated
185 with amino acid and/or protein metabolism (Fig. 3). A total of 97 DEGs were involved in these
186 processes, of which 43 were upregulated in symbiotic animals. Interestingly, the DEGs involved
187 in most of the enriched biological processes exhibited consistent expression changes (Fig. 3A),
188 i.e. the genes associated with the corresponding process were either exclusively upregulated or
189 downregulated.
190

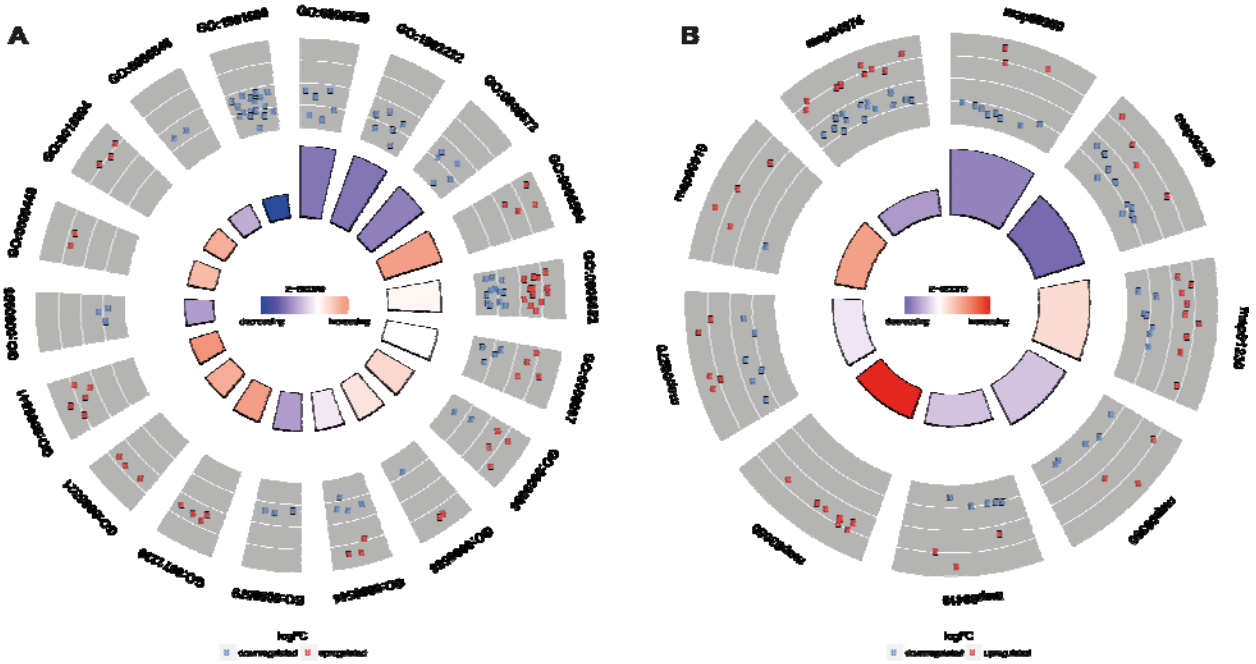

GO	Description
GO:0006559	L-phenylalanine catabolic process
GO:1902222	erythrose 4-phosphate/phosphoenolpyruvate family amino acid catabolic process
GO:0006572	tyrosine catabolic process
GO:0006564	L-serine biosynthetic process
GO:0008652	cellular amino acid biosynthetic process
GO:0000097	sulfur amino acid biosynthetic process
GO:0009086	methionine biosynthetic process
GO:0006566	threonine metabolic process
GO:0006544	glycine metabolic process
GO:0006579	amino acid betaine catabolic process
GO:0071230	cellular response to amino acid stimulus
GO:0006521	regulation of cellular amino acid metabolic process
GO:0006541	glutamine metabolic process
GO:0000098	sulfur amino acid catabolic process
GO:0009448	gamma-aminobutyric acid metabolic process
GO:0015804	neutral amino acid transport
GO:0006546	glycine catabolic process
GO:1901606	alpha-amino acid catabolic process

Map	Description
map00350	Tyrosine metabolism
map00260	Glycine, serine and threonine metabolism
map01230	Biosynthesis of amino acids
map00360	Phenylalanine metabolism
map00410	beta-Alanine metabolism
map03050	Proteasome
map00270	Cysteine and methionine metabolism
map00910	Nitrogen metabolism
map04974	Protein digestion and absorption

FIG 3 Amino acid metabolism biological processes (A) and pathways (B) enriched with DEGs identified in meta-analysis. For the two Circos plots, the height of each bar in the inner circle indicates statistical significance of the enriched GO terms (A) and KEGG pathways (B), while color of the bars represents the overall regulation effect of each process. The outer circle shows the differential expression of genes associated with each process, where red and blue represent upregulation and downregulation in symbiotic anemones, respectively. The table describes the annotation of each term or pathway.

Further integration of these enriched biological processes and pathways revealed an amino acid metabolism hub in *Aiptasia-Symbiodinium* symbiosis (Fig. 4). We observed that genes catalyzing glycine/serine biosynthesis from food-derived choline were systematically downregulated in symbiotic anemones. In contrast, the genes involved in *de novo* serine biosynthesis from 3-phosphoglycerate, one of the glycolysis intermediates, and glutamine/glutamate metabolism were generally upregulated (Fig. 4A). The resulting change in amino acid synthesis pathways suggested that symbiotic hosts utilize glucose and waste ammonium to synthesize serine and glycine, which are both main precursors for many other amino acids (Supplementary Information S1). Based on these findings, we hypothesized that the host uses symbiont-derived glucose to assimilate waste ammonium to produce amino acids.

To test this hypothesis, we further investigated metabolomes of symbiotic and aposymbiotic anemones using nuclear magnetic resonance (NMR) spectroscopy. Three metabolites in the *de novo* serine biosynthesis pathway were highly abundant in symbiotic *Aiptasia* (two of them significantly so, $p < 0.05$), while five out of the six intermediates in the alternative glycine/serine biosynthesis pathway using food-derived choline were significantly enriched in aposymbiotic anemones as predicted (Fig. 4B). However, as glucose produces multiple peaks in the ^{1}H NMR spectrum, and most of these peaks overlap with many other potential metabolites in both symbiotic and aposymbiotic anemones, it was not possible to precisely determine glucose concentrations via NMR. Consequently, we performed ^{13}C bicarbonate labeling experiments and compared metabolite profiles of symbiotic and aposymbiotic anemones using gas chromatography-mass spectrometry (GC-MS), in order to test if the glucose is indeed provided by the symbiont and if the downstream usage of symbiont derived organic carbon is in the host. Our experiments confirmed that symbionts provide large amounts of ^{13}C-labeled glucose to the

host (Fig. S3) and that the ^{13}C-labeling was significantly enriched in many amino acids and their precursors in symbiotic anemones compared to aposymbiotic ones (Table S2). Moreover, metabolite set enrichment analysis indicates that these ^{13}C-enriched are associated mainly with several amino acid metabolism pathways (Fig. S4), which is consistent with the enrichment analysis of 731 differentially expressed genes. For the amino acids with good abundance in both symbiotic and aposymbiotic animals, we examined the proportion of ^{13}C in each of them, respectively. Interestingly, we observed relatively stable increases (~1.5-fold) of ^{13}C levels in symbiotic animals compared with aposymbiotic ones (Fig. 4C). This constant increase may indicate there is a unique carbon source (photosynthesis-produced glucose) rather than multiple sources (glucose and symbiont-derived amino acids) in host amino acid biosynthesis.

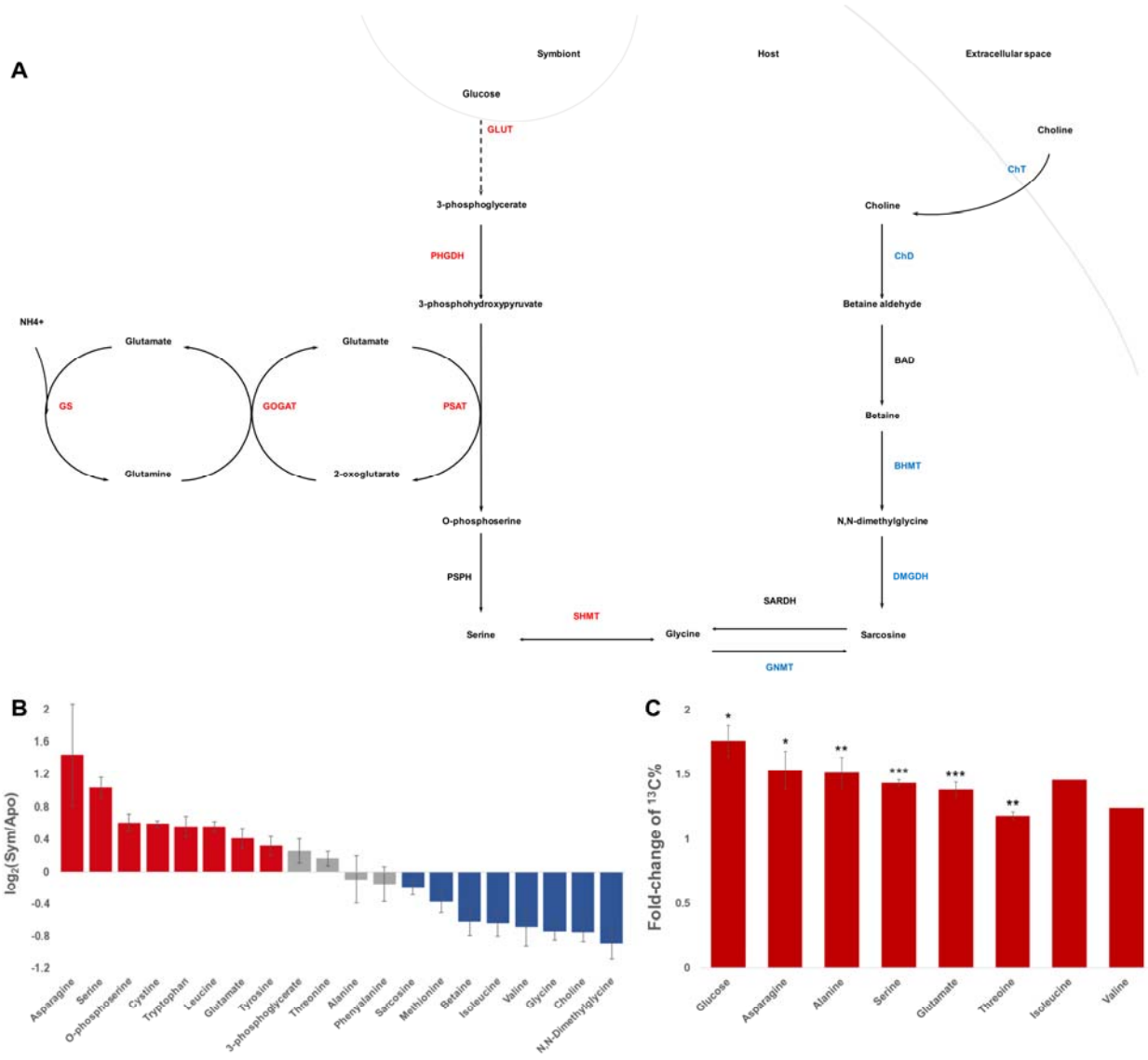

FIG 4 Amino acid metabolism in *Aiptasia-Symbiodinium* symbiosis. (A) Serine biosynthesis in *Aiptasia* with different symbiotic states. The pathway on the left indicates *de novo* serine biosynthesis from symbiont-produced glucose, while the right part represents glycine/serine biosynthesis from food-derived choline. Enzyme names are colored to indicate differential expression of the corresponding genes, where red and blue mean upregulation and downregulation in symbiotic anemones, respectively. (B) Metabolite abundance changes in response to symbiosis. Color represent abundance changes, with red for significant increases in symbiotic anemones, blue for significant increase in aposymbiotic animals, and gray for non-

significant changes. (C) Increasing ^{13}C proportion of glucose and amino acids in symbiotic *Aiptasia*. Asterisks denote statistical significance of the changes (two-tail *t* test: * $p < 0.05$, ** $p < 0.01$, *** $p < 0.001$). Statistical testing of isoleucine and valine was not possible as they were detected in only one aposymbiotic replicate with reasonable concentration. Error bar represents standard error of the mean.

Discussion

Batch effects are known to introduce strong variation in high throughput sequencing studies[28, 29]. However, this is often overlooked in transcriptomic studies, and especially so in non-model organisms. Our analysis of RNA-Seq data from four independent experiments analyzing transcriptional changes between symbiotic and aposymbiotic *Aiptasia* highlighted that batch effects are indeed pervasive in published data, even among studies using the same genotype (clonal strain CC7). Analyses of the combined dataset from all four experiments showed clear grouping of samples by experiment rather than treatment. However, when each experiment was analyzed independently, replicates separated by symbiotic states as expected. Interestingly, we found that the observed batch effects were not restricted to technical biases. Our analyses showed that the specific experimental setups in each study were a greater source of variance than the symbiosis state, which was the actual factor of interest in these studies. More importantly, we found that genes closely related to the processes involved in symbiosis, such as nutrient exchanges, may also respond significantly to various parameters of culture conditions, such as the feeding frequency, days between sampling and feeding, water, light intensity, and the temperature. Without careful design, such factors may exert effects on gene expression that mask the changes specific to the treatment of interest (symbiotic state).

Based on our findings, we suggest two potential venues to reduce the high signal-to-noise ratio in differential expression studies. Firstly, future transcriptomic efforts should take extreme care to standardize all experimental conditions save for the one under study. For example, culture conditions should be identical, treatments should be performed on multiple independent batches, RNA extractions and library preparation should be carried out on all samples simultaneously. The prepared libraries should also be sequenced in the same run to further minimize technical variations. Secondly, one should not dogmatically adhere to the convention of using $p = 0.05$ as the cutoff for statistical significance. If a study considers one in every three genes as significantly differentially expressed, to a careful reader, the proclaimed significance of those genes is diminished. As the number of DEGs increase, the rate of type I errors would also increase, which would make the discovery of meaningful biological processes more difficult.

From the functional interpretation of DEGs associated with enriched GO terms and KEGG pathways, we found that many processes in the host were significantly induced or suppressed in response to symbiosis. One of the key features that has been overlooked in previous studies is the switch of serine biosynthesis pathways in *Aiptasia* in response to symbiosis.

The downregulation of choline transport indicates a decrease of the host's demand on dietary choline during symbiosis. Correspondingly, genes involved in the downstream conversion of choline to betaine and the production of glycine from betaine are also downregulated. The decrease of glycine caused by this downregulation is likely compensated by the metabolism of serine, which can be achieved by the observed upregulation of serine hydroxymethyltransferase (SHMT, AIPGENE4781), which catalyzes the interconversions between glycine and serine. Interestingly, our results suggest that serine is one of the key components in the amino acid interconversions, as the genes involved in its *de novo* biosynthesis from 3-phosphoglycerate (one

289 of the intermediates of glycolysis) were consistently upregulated. The conversion from glutamate
290 to 2-oxoglutarate, catalyzed by the upregulated phosphoserine aminotransferase (PSAT,
291 AIPGENE17104), may serve as the main reaction to provide amino groups for the biosynthesis
292 of amino acids. Since 2-oxoglutarate is also one of the intermediates in the citrate acid cycle, an
293 increase of glucose provided by the symbionts may also increase the overall activity of the cycle,
294 hence raising the relative abundance of 2-oxoglutarate in symbiotic animals. High levels of 2-
295 oxoglutarate have been reported to induce ammonium assimilation through glutamine synthetase
296 / glutamate synthase cycle[30]. Consistent with this finding, we observe all the genes involved in
297 this pathway to be upregulated in symbiotic anemones.
298 Metabolomic analyses of symbiotic and aposymbiotic anemones confirm the predictions derived
299 from our transcriptomic meta-analysis. Most of the intermediates in the *de novo* serine
300 biosynthesis using symbiont-derived glucose were highly enriched in symbiotic anemones and
301 showed increased ^{13}C-labeling. whereas many of the metabolites from choline-betaine-glycine-
302 serine conversion have decreased abundance in symbiotic animals. Furthermore, we also
303 identified many other amino acids showing significantly increased abundance and ^{13}C-labeling
304 signals, suggesting that serine may serves as metabolic intermediate for the production of other
305 amino acids. Taken together, these results highlight that symbiont-derived glucose fuels
306 ammonium assimilation and amino acid production in the host and that serine biosynthesis acts
307 as a main metabolic hub in symbiotic hosts.
308 The strong shifts in host amino acids metabolic pathways induced by symbiont-provided glucose
309 described here indicate the major nitrogen and carbon sources of the anemone host, and their
310 interactions in the *Aiptasia-Symbiodinium* symbiosis. The catabolism of glucose through
311 pathways such as glycolysis, pentose phosphate pathway, and citric acid cycle, not only

312 generates more energy (in forms of ATP, NADH, and NADPH), which is critical to ammonium
313 assimilation, but also produces more intermediate metabolites that can serve as carbon
314 backbones in many biosynthetic pathways such as amino acid synthesis. Our findings thus
315 highlight nitrogen conservation, i.e. the host driven assimilation of waste ammonium using
316 symbiont-derived carbon, as a central mechanism of the cnidarian-algal endosymbiosis[16]. This
317 metabolic interaction might serve as a self-regulating mechanism for the host to control symbiont
318 density through the regulation of nitrogen availability[15] in a carbon dependent manner. This
319 allows for higher nitrogen availability in early stages of infection (few symbionts translocating
320 few carbon) and gradual reduction of nitrogen availability with increasing symbiont densities
321 (many symbionts translocating more carbon). The strict dependence of this mechanism on
322 symbiont-derived carbon highlights the sensitivity of this relationship to changes in carbon
323 translocation as imposed by stress-induced retention of photosynthates by symbionts[31, 32].
324

Materials and Methods

Data collection and pre-processing. Based on literature review of recently published *Aiptasia* genome and transcriptome studies, four datasets generated from three previous publications[2, 24, 26] were obtained (Table 1). All RNA-Seq experiments were performed on the clonal *Aiptasia* strain (CC7) and sequenced on the same platform (Illumina HiSeq 2000). Three of the datasets contained 101 bp paired-end reads, while the last one contained 36 bp single-end reads. Samples were labeled based on the initials of the first author of published papers and ongoing project.

As all raw data from Lehnert et al.[24] was provided as a monolithic FASTQ file, a custom Python script was written to split the reads into its constituent replicates, as inferred from the FASTQ annotation lines.

Table 1 Summary of the NGS data sources used in this study

Sample	Source Project	Symbiont	Library	Accession Number
Apo-YL[26]		None	101-bp, paired-end	
Sym-YL[26]		Symbiodinium SSB01	101-bp, paired-end	
Apo-SB[2]	*Aiptasia* genome, PRJNA261862	None	101-bp, paired-end	SRR1648359, SRR1648360, SRR1648361, SRR1648362
Sym-SB[2]	*Aiptasia* genome, PRJNA261862	Symbiodinium SSB01	101-bp, paired-end	SRR1648369, SRR1648370, SRR1648371, SRR1648372
Apo-EML[24]	*Aiptasia pallida* Transcriptome, PRJNA159215	None	101-bp, paired-end	SRR696732
Sym-EML[24]	*Aiptasia pallida* Transcriptome, PRJNA159215	Native *Symbiodinium* strain	101-bp, paired-end	SRR612165
Apo-EML-36[24]	*Aiptasia pallida* Transcriptome, PRJNA159215	None	36-bp, single-end	SRR612167

Sym-EML-36[24]	*Aiptasia pallida* Transcriptome, PRJNA159215	Native *Symbiodinium* strain	36-bp, single-end	SRR612166

Identification of DEGs. To avoid biases stemming from the use of disparate bioinformatics tools in calling DEGs, data from the four datasets were processed with identical analytical pipelines.

Gene expressions were quantified (in TPM, transcripts per million) based on the published *Aiptasia* gene models[2] using kallisto v0.42.4[33]. DEGs were independently identified in the four datasets using sleuth v0.28.0[34]. Genes with corrected p values < 0.05 were considered differentially expressed.

To enable direct comparisons of gene expression values between datasets, another normalization with sleuth was carried out on all samples ($n = 17$ aposymbiotic and $n = 17$ symbiotic). Principal component analysis (PCA) and ranked correlation analysis (RCA) were carried out on these normalized expression values to assess the relationship between samples and reproducibility of these studies.

Profiling sources of batch effects. Principal variance components analysis (PVCA), a technique that was developed to estimate the extent of batch effects in microarray experiments[27], was used several times in our study. A PVCA was carried out on raw data to estimate the batch effects in the combined dataset and their possible source in the original experimental designs; similarly, the normalized data was also assessed for the reduction of batch effects post-normalization. We also performed PVCA on normalized expression values of the differentially expressed genes (DEG) identified in each independent analysis or the final meta-analysis to detect the robustness of DEG calling.

Meta-analysis across studies. For every gene with at least two studies with significant differential expression values, a meta-analysis was performed to determine the overall effect size and associated standard error. Effect sizes from each study i (represented as w_i) were calculated as the natural logarithm of its expression ratio ($\ln R_i$), i.e. geometric means of all expression values in the aposymbiotic state divided by the geometric means of all expression values in the symbiotic state. Conveniently, this value is approximately equal to the β_i value provided by sleuth. As sleuth also calculates the standard error of β_i, the variance of $\ln R_i$ was not calculated via the typical approximation—instead, the variance v_i was directly calculated as

$$v_i = SE_{\beta_i}^2 \cdot n_i$$

where n_i represents the number of replicates in study i.

To combine the studies, a random-effects model was used. While the use of this model is somewhat discouraged for meta-analyses with few studies as it is prone to produce type I errors[35], we still opted for its use over the fixed-effects model due to the substantial inter-study variation evident in the PCAs performed previously. Also, the type I error rate could be controlled by setting a more conservative p threshold, if required.

372 The DerSimonian and Laird [36] method was implemented as described below. Studies with
373 individual effect sizes m_i were weighted (w^*) by a combination of the between-study variation
374 (τ^2) and within-study variation (v_i), according to the formula

$$w_i^* = \frac{1}{v_i + \tau^2}$$

375 The between-study variation (τ^2) across all *k* studies was calculated as

$$\tau^2 = \max\left\{\frac{Q - df}{C}, 0\right\}$$

376 where

$$Q = \sum w_i (T_i - \bar{T})^2$$

$$C = \sum w_i - \frac{\sum w_i^2}{\sum w_i}$$

377 The weighted mean (m^*) was calculated as

$$m^* = \frac{\sum w_i^* T_i}{\sum w_i^*}$$

378 while the standard error of the combined effect was

$$SE(m^*) = \frac{1}{\sqrt{\sum w_i^*}}$$

379 The two-tailed p-value was calculated using

$$p = 2\left[1 - \Phi\left(\left|\frac{m^*}{SE(m^*)}\right|\right)\right]$$

380 and then subsequently corrected for multiple hypothesis testing with the Benjamini-Hochberg-
381 Yekutieli procedure[37, 38] using a Python script. Genes with corrected $p < 0.05$ were considered
382 differentially expressed. For transparency, calculations for all equations were implemented
383 manually in Microsoft Excel (Table S3) following established guidelines[39].

Functional interpretation of DEGs. Gene ontology (GO) and KEGG pathway enrichment analyses were both conducted on five DEG lists: one each from the four independent datasets, and one from the results of the meta-analysis.

Identification of enriched GO terms were conducted using topGO[40] by a self-developed R script (https://github.com/lyijin/topGO_pipeline). A GO term was considered enriched only when its *p* value was less than 0.05.

KEGG pathway enrichment analyses were performed using Fisher's exact and subsequent multiple testing correction via false discovery rate (FDR) estimation. A KEGG pathway was deemed enriched (or depleted) only when its FDR less than 0.05. The results of enrichment analyses were visualized using GOplot[41].

Metabolomic profiles of symbiotic and aposymbiotic anemones. *Aiptasia* strain CC7 was bleached and re-infected with a compatible strain of *Symbiodinium* SSB01 as previously reported[2]. All the symbiotic and aposymbiotic anemones were maintained in the laboratory in autoclaved seawater (ASW) at 25 °C in 12-hour light/12-hour dark cycle with light intensity of ~30 μmol photons $m^{-2}s^{-1}$ for over three years. Anemones were fed three times a week with freshly hatched *Artemia* nauplii, and water change was done on the day after feeding.

Anemones were rinsed extensively to remove any external contaminations, and starved for two days in ASW and transferred into ASW with 10 mM ^{13}C-labelled sodium bicarbonate (Sigma-Aldrich, USA) for another two days before sampling. The four-day starvation period ensured all *Artemia* had been digested and consumed, hence there was no contamination from *Artemia* in the samples for NMR and GC-MS. The samples were drained completely on clean tissues to remove any water on surface, then snap frozen in liquid nitrogen to avoid any further metabolite changes in downstream processing.

To compare metabolomic profiles of anemones at different symbiotic states, four replicates of each state (*n* = 30 individuals per replicate), were processed for metabolite extraction using a previously reported methanol/chloroform method[42]. The free amino acid-containing methanol phase was dried using CentriVap Complete Vacuum Concentrators (Labconco, USA).

For NMR metabolite profiling, samples were dissolved in 600 µl of deuterated water (D_2O), and vortexed vigorously for at least 30 seconds. Subsequently, 550 µL of the solution was transferred to 5 mm NMR tubes. NMR spectrum was recorded using 700 MHz AVANCE III NMR spectrometer equipped with Bruker CP TCI multinuclear *CryoProbe* (BrukerBioSpin, Germany). To suppress any residual HDO peak, the ^{1}H NMR spectrum were recorded using excitation sculpting pulse sequence (zgesgp) program from Bruker pulse library. To achieve a good signal-to-noise ratio, each spectrum was recorded by collecting 512 scans with a recycle delay time of 5 seconds digitized into 64 K complex data points over a spectral width of 16 ppm. Chemical shifts were adjusted using 3-trimethylsilylpropane-1-sulfonic acid as internal chemical shift reference. Before Fourier transformations, the FID values were multiplied by an exponential function equivalent to a 0.3 Hz line broadening factor. The data was collected and quantified using Bruker Topspin 3.0 software (Bruker BioSpin, Germany), with metabolite-peak assignment using Chenomx NMR Suite v8.3, with an up-to-date reference library (Chenomx Inc., Canada).

For ^{13}C-labelling investigation using GC-MS, dried samples were re-dissolved in 50 µl of Methoxamine (MOX) reagent (Pierce, USA) at room temperature and derivatized at 60 °C for one hour. 100 µl of *N,O-bis*-(trimethylsilyl) trifluoroacetamide (BSTFA) was added and incubated at 60 °C for further 30 min. 2 µl of the internal standard solution of fatty acid methyl ester (FAME) were then spiked in each sample and centrifuged for 5 min at 10,000 rpm. 1 µl of the derivatized solution was analyzed using single quadrupole GC-MS system (Agilent 7890

GC/5975C MSD) equipped with EI source at ionization energy of 70 eV. The temperature of the ion source and mass analyzer was set to 230 °C and 150 °C, respectively, and a solvent delay of 9.0 min. The mass analyzer was automatically tuned according to manufacturer's instructions, and the scan was set from 35 to 700 with scan speed 2 scans/s. Chromatography separation was performed using DB-5MS fused silica capillary column (30m x 0.25 mm I.D., 0.25 µm film thickness; Agilent J&W Scientific, USA), chemically bonded with 5% phenyl 95% methylpolysiloxane cross-linked stationary phase. Helium was used as the carrier gas with constant flow rate of 1.0 ml min^{-1}. The initial oven temperature was held at 80□C for 4 min, then ramped to 300 °C at a rate of 6.0 °C min-1, and held at 300 °C for 10 min. The temperature of the GC inlet port and the transfer line to the MS source was kept at 200 °C and 320 °C, respectively. 1 µl of the derivatized solution of the sample was injected into split/splitless inlet using an auto sampler equipped with 10 µl syringe. The GC inlet was operated under splitless mode. Metabolites in all samples were identified using Automated Mass Spectral Deconvolution and Identification System software (AMDIS) with the NIST special database 14 (National Institute of Standards and Technology, USA). The mass isotopomer distributions (MIDs) of all compounds were detected and their ^{13}C-labelling enrichment in symbiotic *Aiptasia* were investigated using MIA[43]. Pathways associated with these ^{13}C-enriched metabolites were explored using MetaboAnalyst v3.0[44].

Author Contributions

M.A. conceived the project. G.C., Y.J.L., M.A., Y.L., N.I.Z., and V.M.E. collected the RNA-Seq data, performed data analyses, and visualized the results. G.C., N.K., A.E., and M.A. conducted

452 metabolomic experiments and analyzed the data. G.C., Y.J.L., and M.A. wrote the manuscript
453 with method input from other authors. All authors have read and agreed on the final draft.
454
455 **Acknowledgements**
456 We would like to thank Jit Ern Chen and Maha J. Cziesielski for valuable comments on our
457 manuscript. This publication is based upon work supported by the King Abdullah University of
458 Science and Technology (KAUST) Office of Sponsored Research (OSR) under Award No.
459 URF/1/2216-01.

References

1. Roth MS. The engine of the reef: photobiology of the coral–algal symbiosis. *Microbial Symbioses* **5**, 422 (2014).

2. Baumgarten S, *et al.* The genome of Aiptasia, a sea anemone model for coral symbiosis. *Proc Natl Acad Sci U S A* **112**, 11893-11898 (2015).

3. Grajales A, Rodriguez E. Morphological revision of the genus Aiptasia and the family Aiptasiidae (Cnidaria, Actiniaria, Metridioidea). *Zootaxa* **3826**, 55-100 (2014).

4. Lehnert EM, Burriesci MS, Pringle JR. Developing the anemone Aiptasia as a tractable model for cnidarian-dinoflagellate symbiosis: the transcriptome of aposymbiotic A. pallida. *BMC Genomics* **13**, 271 (2012).

5. Clayton WS, Lasker HR. Individual and population growth in the asexually reproducing anemone Aiptasia pallida Verrill. *J Exp Mar Bio Ecol* **90**, 249-258 (1985).

6. Grawunder D, Hambleton EA, Bucher M, Wolfowicz I, Bechtoldt N, Guse A. Induction of Gametogenesis in the Cnidarian Endosymbiosis Model Aiptasia sp. *Sci Rep* **5**, 15677 (2015).

7. Kinzie RA, 3rd, Takayama M, Santos SR, Coffroth MA. The adaptive bleaching hypothesis: experimental tests of critical assumptions. *Biol Bull* **200**, 51-58 (2001).

8. Perez S, Weis V. Nitric oxide and cnidarian bleaching: an eviction notice mediates breakdown of a symbiosis. *J Exp Biol* **209**, 2804-2810 (2006).

9. Belda-Baillie CA, Baillie BK, Maruyama T. Specificity of a model cnidarian-dinoflagellate symbiosis. *Biol Bull* **202**, 74-85 (2002).

10. Burriesci MS, Raab TK, Pringle JR. Evidence that glucose is the major transferred metabolite in dinoflagellate–cnidarian symbiosis. *J Exp Biol* **215**, 3467-3477 (2012).

11. Pogoreutz C, Radecker N, Cardenas A, Gardes A, Voolstra CR, Wild C. Sugar enrichment provides evidence for a role of nitrogen fixation in coral bleaching. *Glob Chang Biol* **23**, 3838-3848 (2017).

12. Rädecker N, Pogoreutz C, Voolstra CR, Wiedenmann J, Wild C. Nitrogen cycling in corals: the key to understanding holobiont functioning? *Trends Microbiol* **23**, 490-497 (2015).

13. Aranda M, *et al.* Genomes of coral dinoflagellate symbionts highlight evolutionary adaptations conducive to a symbiotic lifestyle. *Sci Rep* **6**, 39734 (2016).

14. Muscatine L, Falkowski PG, Dubinsky Z, Cook PA, McCloskey LR. The Effect of External Nutrient Resources on the Population Dynamics of Zooxanthellae in a Reef

Coral. *Proceedings of the Royal Society of London B: Biological Sciences* **236**, 311-324 (1989).

15. Falkowski PG, Dubinsky Z, Muscatine L, McCloskey L. Population Control in Symbiotic Corals. *Bioscience* **43**, 606-611 (1993).

16. Wang J, Douglas AE. Nitrogen recycling or nitrogen conservation in an alga-invertebrate symbiosis? *J Exp Biol* **201**, 2445-2453 (1998).

17. Barneah O, Benayahu Y, Weis VM. Comparative proteomics of symbiotic and aposymbiotic juvenile soft corals. *Mar Biotechnol* **8**, 11-16 (2006).

18. deBoer ML, Krupp DA, Weis VM. Proteomic and transcriptional analyses of coral larvae newly engaged in symbiosis with dinoflagellates. *Comp Biochem Physiol Part D Genomics Proteomics* **2**, 63-73 (2007).

19. Kuo J, Chen M-C, Lin C-H, Fang L-S. Comparative gene expression in the symbiotic and aposymbiotic Aiptasia pulchella by expressed sequence tag analysis. *Biochem Biophys Res Commun* **318**, 176-186 (2004).

20. Rodriguez-Lanetty M, Phillips WS, Weis VM. Transcriptome analysis of a cnidarian-dinoflagellate mutualism reveals complex modulation of host gene expression. *BMC Genomics* **7**, 23 (2006).

21. Voolstra CR, *et al.* The host transcriptome remains unaltered during the establishment of coral–algal symbioses. *Mol Ecol* **18**, 1823-1833 (2009).

22. Weis VV, Levine R. Differential protein profiles reflect the different lifestyles of symbiotic and aposymbiotic Anthopleura elegantissima, a sea anemone from temperate waters. *J Exp Biol* **199**, 883-892 (1996).

23. Yuyama I, Watanabe T, Takei Y. Profiling differential gene expression of symbiotic and aposymbiotic corals using a high coverage gene expression profiling (HiCEP) analysis. *Mar Biotechnol* **13**, 32-40 (2011).

24. Lehnert EM, Mouchka ME, Burriesci MS, Gallo ND, Schwarz JA, Pringle JR. Extensive Differences in Gene Expression Between Symbiotic and Aposymbiotic Cnidarians. *G3: Genes|Genomes|Genetics* **4**, 277-295 (2014).

25. Oakley CA, Ameismeier MF, Peng L, Weis VM, Grossman AR, Davy SK. Symbiosis induces widespread changes in the proteome of the model cnidarian Aiptasia: Symbiosis and the Aiptasia proteome. *Cell Microbiol* **18**, 1009-1023 (2015).

26. Li Y, *et al.* DNA methylation regulates transcriptional homeostasis of algal endosymbiosis in the coral model Aiptasia. *bioRxiv,* (2017).

552 27. Li J, Bushel PR, Chu T-M, Wolfinger RD. Principal Variance Components Analysis:
553 Estimating Batch Effects in Microarray Gene Expression Data. In: *Batch Effects and*
554 *Noise in Microarray Experiments* (ed^(eds). John Wiley & Sons, Ltd (2009).
555
556 28. Leek JT, *et al.* Tackling the widespread and critical impact of batch effects in high-
557 throughput data. *Nat Rev Genet* **11**, 733-739 (2010).
558
559 29. Peixoto L, *et al.* How data analysis affects power, reproducibility and biological insight
560 of RNA-seq studies in complex datasets. *Nucleic Acids Res* **43**, 7664-7674 (2015).
561
562 30. Cabello P, Roldan MD, Moreno-Vivian C. Nitrate reduction and the nitrogen cycle in
563 archaea. *Microbiology* **150**, 3527-3546 (2004).
564
565 31. Baker DM, Freeman CJ, Wong JCY, Fogel ML, Knowlton N. Climate change promotes
566 parasitism in a coral symbiosis. *ISME J*, (2018).
567
568 32. Matthews JL, *et al.* Optimal nutrient exchange and immune responses operate in partner
569 specificity in the cnidarian-dinoflagellate symbiosis. *Proc Natl Acad Sci U S A* **114**,
570 13194-13199 (2017).
571
572 33. Bray NL, Pimentel H, Melsted P, Pachter L. Near-optimal probabilistic RNA-seq
573 quantification. *Nat Biotechnol* **34**, 525-527 (2016).
574

34. Pimentel H, Bray NL, Puente S, Melsted P, Pachter L. Differential analysis of RNA-seq incorporating quantification uncertainty. *Nat Methods* **14**, 687-690 (2017).

35. Guolo A, Varin C. Random-effects meta-analysis: the number of studies matters. *Stat Methods Med Res* **26**, 1500-1518 (2017).

36. DerSimonian R, Laird N. Meta-analysis in clinical trials. *Control Clin Trials* **7**, 177-188 (1986).

37. Benjamini Y, Hochberg Y. Controlling the False Discovery Rate: A Practical and Powerful Approach to Multiple Testing. *Journal of the Royal Statistical Society Series B (Methodological)* **57**, 289-300 (1995).

38. Benjamini Y, Yekutieli D. The control of the false discovery rate in multiple testing under dependency. *Ann Stat* **29**, 1165-1188 (2001).

39. Borenstein M, Hedges LV, Higgins JPT, Rothstein HR. Random-Effects Model. In: *Introduction to Meta-Analysis* (ed^(eds). John Wiley & Sons, Ltd (2009).

40. Alexa A, Rahnenfuhrer J. topGO: enrichment analysis for gene ontology. *R package version*, (2010).

41. Walter W, Sanchez-Cabo F, Ricote M. GOplot: an R package for visually combining expression data with functional analysis. *Bioinformatics* **31**, 2912-2914 (2015).

42. Lin CY, Wu HF, Tjeerdema RS, Viant MR. Evaluation of metabolite extraction strategies from tissue samples using NMR metabolomics. *Metabolomics* **3**, 55-67 (2007).

43. Weindl D, Wegner A, Hiller K. MIA: non-targeted mass isotopolome analysis. *Bioinformatics* **32**, 2875-2876 (2016).

44. Xia J, Sinelnikov IV, Han B, Wishart DS. MetaboAnalyst 3.0--making metabolomics more meaningful. *Nucleic Acids Res* **43**, W251-257 (2015).